

# A Unified Framework for Simulating Strongly-Coupled Fluid-Robot Multiphysics

Jeong Hun Lee<sup>1</sup>, Junzhe Hu<sup>1</sup>, Sofia Kwok<sup>1</sup>, Carmel Majidi<sup>1</sup>, and Zachary Manchester<sup>1</sup>

**Abstract**—We present a framework for simulating fluid-robot multiphysics as a single, unified optimization problem. The coupled manipulator and incompressible Navier-Stokes equations governing the robot and fluid dynamics are derived together from a single Lagrangian using the principle of least action. We then employ discrete variational mechanics to derive a stable, implicit time-integration scheme for jointly simulating both the fluid and robot dynamics, which are tightly coupled by a constraint that enforces the no-slip boundary condition at the fluid-robot interface. Extending the classical immersed boundary method, we derive a new formulation of the no-slip constraint that is numerically well-conditioned and physically accurate for multibody systems commonly found in robotics. We demonstrate our approach’s physical accuracy on benchmark computational fluid-dynamics problems, including Poiseuille flow and a disc in free stream. We then design a locomotion policy for a novel swimming robot in simulation and validate results on real-world hardware, showcasing our framework’s sim-to-real capability for robotics tasks.

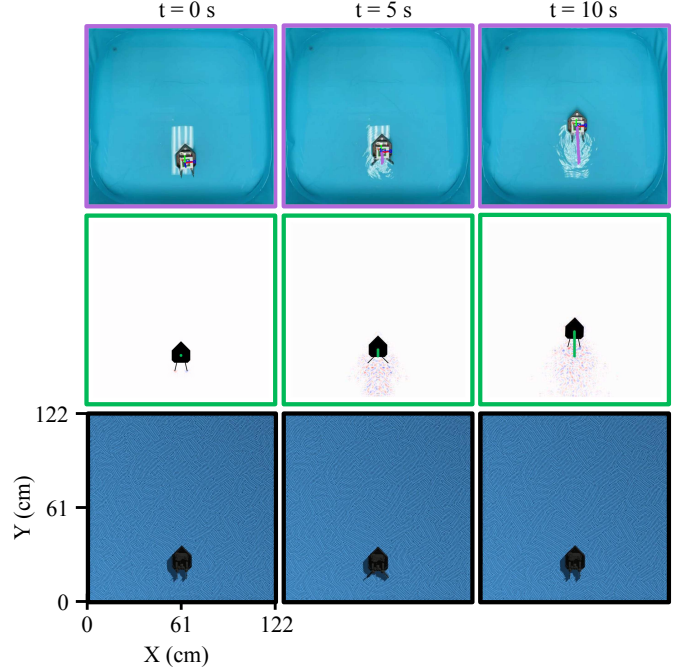
**Index Terms**—Robotics, Simulation, Multiphysics, Fluid-Structure Interaction

## I. INTRODUCTION

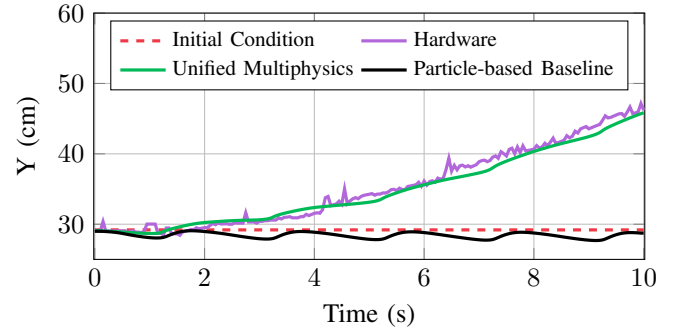
In recent years, there has been considerable interest in designing robot control policies in multiphysics settings such as deformable-object manipulation [1]–[3], fluid transport [4], [5], and locomotion [6]–[8]. However, real-world data collection and training in such complex environments presents a major challenge. As a result, multiphysics-simulation platforms [9], [10] have seen growing interest and ongoing development, with many robotics applications still lacking viable physics engines.

One such application is bio-inspired locomotion for underwater vehicles [11]–[16], which has garnered attention for its energy efficiency and high degree of maneuverability [17]–[19]. Although various bioinspired hardware designs have been introduced [14], [20]–[22], relatively little work has been done to make these vehicles operate autonomously with the same performance as their biological counterparts [21]. We attribute this to the difficulty of modeling and simulating such systems, where both whole-body robot dynamics and complex fluid-structure interaction (FSI) are present as shown in Figure 2.

We propose a unified framework for jointly deriving and simulating fluid-robot multiphysics. Specifically, we formulate the combined Lagrangian using the principle of least action to model the multiphysics as a single continuous-time optimization problem, from which we derive the coupled



(a) Trajectory visualizations of the robot executing a forward-swimming gait. The top row shows the real robot, while the middle row is our method and the bottom row is a particle-based simulation.



(b) Time history of the robot position in the corresponding forward-swimming direction.

Fig. 1: Sim-to-real validation of a squid-like robot executing an open-loop swimming gait in initially-still water. Our unified-multiphysics approach (green) is able to model the propulsion resulting from the fluid-robot interaction unlike the particle-based baseline in Genesis (black)

incompressible Navier-Stokes and manipulator equations as depicted in Figure 3. We show that the multiphysics coupling stems from a constraint that enforces the no-slip boundary condition at the fluid-robot interface. We then employ discrete variational mechanics [23] to discretize the unified action

<sup>1</sup> The Robotics Institute, Carnegie Mellon University, Pittsburgh, USA  
jeonghunlee@cmu.edu, junzhehu@andrew.cmu.edu,  
sofiak@andrew.cmu.edu, carmel.majidi@cmu.edu,  
zacm@cmu.edu

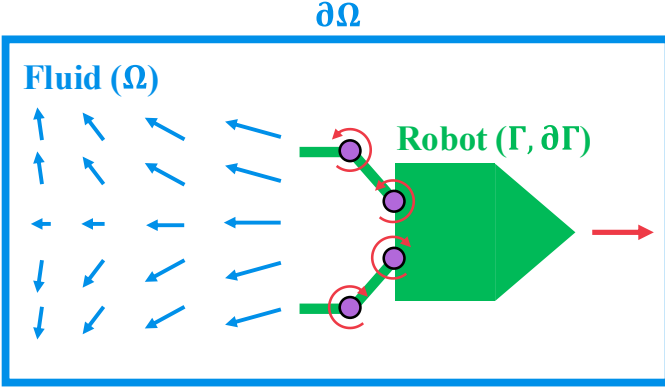


Fig. 2: An overview of the multiphysics problem we address, in which a controlled robotic system must interact with the surrounding incompressible Newtonian fluid (e.g., water) to swim. We denote the fluid domain as  $\Omega$  and its boundary  $\partial\Omega$ .  $\Gamma$  and  $\partial\Gamma$  correspond to the robot geometry and its boundary.

directly, which results in an implicit time-integration scheme that naturally simulates the robot and fluid dynamics in a stable, coupled manner. We also extend the immersed boundary method from the computational fluid dynamics (CFD) literature [24], [25] to derive an integral “weak-form” version of the no-slip constraint that is amenable to multibody robotic systems. We benchmark our approach on various classical CFD problems including Poiseuille flow and a disc in free stream. We additionally showcase our approach’s ability to model an actuated robotic system, specifically a novel squid-inspired robot. We validate our simulation results on real-world hardware, showcasing the sim-to-real capabilities of our framework. In summary, our contributions are:

- A unified representation for strongly-coupled fluid-robot multiphysics via the principle of least action.
- An extension of variational integration for simulating multiphysics in the full state space of a robot.
- A new formulation of the no-slip constraint for multibody robotic systems for accurate coupling at the fluid-robot interface.
- Demonstration of our approach in simulation with hardware validation on a bioinspired swimming robot.

The remainder of this paper is organized as follows: In Section II, we provide a literature review on existing fluid-robot interaction simulators, variational mechanics, and computational fluid dynamics solvers. In Section III, we provide an overview of relevant background material on the least action principle, variational integrators, and the immersed-boundary method. Section IV then describes our proposed approach for posing and simulating the coupled fluid-robot physics. In Section V, we provide simulation results on various benchmark problems, including Poiseuille flow and a disc in free stream. We then showcase the sim-to-real-transfer capabilities of our framework on a novel, squid-like swimming robot. In Section VII we provide final concluding remarks and discuss future work to address current limitations.

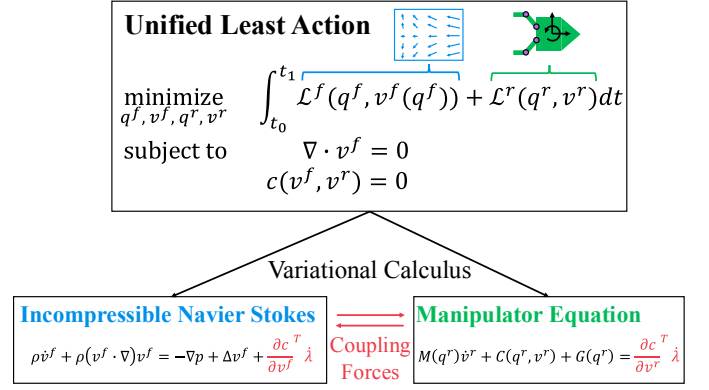


Fig. 3: An overview of our multiphysics model, in which the unified Lagrangian governing the coupled fluid-robot dynamics is formulated using the principle of least action. Rather than the individual differential equations, the combined action is discretized directly to achieve consistent tightly coupled simulation.

## II. RELATED WORKS

### A. Multiphysics Simulation for Robotics

Multiphysics simulators for robotics [9], [10] have garnered recent interest for simulating a diverse range of scenes beyond classical rigid-body dynamics, such as rigid-soft-body interactions for deformable-object manipulation [26] and liquid pouring [27]. These simulators generally employ methods originating from the graphics and particle-based CFD community [28], [29], leveraging their parallelizability and visual-rendering capabilities. However, due to their Lagrangian (i.e., particle-based) representations, these simulators are tailored towards fluid-transport tasks (e.g., liquid pouring) commonly found in robot manipulation. Compared to their Eulerian (grid-based) counterparts, these fluid simulators are currently unable to simulate complex boundary conditions (e.g., free stream) and become intractable when the fluid must be modeled as a continuum. We showcase the limitation of these particle-based simulators for a setting where a robot must operate in an immersive fluid environment. We subsequently pose the robot-fluid multiphysics to account for the respective Lagrangian and Eulerian representations to accurately simulate swimming robots.

### B. Fluid-Structure Interaction (FSI)

Modeling fluid-structure interaction has long been of interest in the CFD community [30]–[33] with the methodologies and results tailored towards single-body systems. Meanwhile results for more complex multibody systems commonly found in robotics have yet to be fully realized [34]. Previous works have simplified the fluid dynamics to potential [16] or Stokes flow [35]–[37] for low-Reynolds-number regimes. Nava et al. proposed a physics-informed, neural-network model of FSI for the optimization of soft robotic swimmers [31]; however, no guarantees can be given when generalizing to new shapes and flow conditions. As a result, Lee et al. [33] proposed a differentiable incompressible-Navier-Stokes-based simulator for robotics called Aquarium. However, Aquarium currently

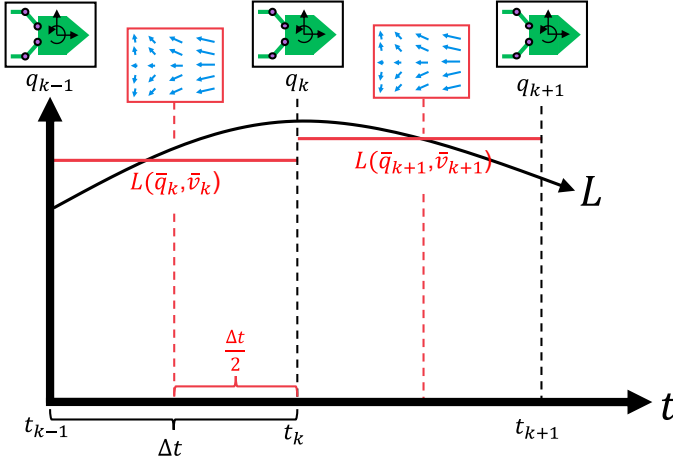


Fig. 4: A midpoint variational integrator, where a quadrature rule is traditionally used to discretize the time integral of Figure 3 to simulate robot configurations,  $q_k$ . However, the fluid is represented as a velocity field,  $\bar{v}_k$  that is approximated at the midpoint, causing a temporal mismatch. Therefore a new variational integrator is formulated for the fluid-robot multiphysics.

does not jointly solve the fluid and robot dynamics and relies on a separate solver to obtain the robot states. It additionally relies on the classical immersed boundary method to represent the robot geometry, which is tailored towards single-body systems. Therefore, we aim to formulate a unified representation of the multiphysics to achieve tightly coupled, generalizable simulation of multibody robots in higher-Reynolds-number fluid environments.

### C. Variational Mechanics for Simulation

Over the past two decades, variational integrators have been developed for accurate simulations of various physical systems [23], [38], [39]. Specifically, variational integrators discretize the least-action principle from which the governing equations of motion are derived. The result is stable simulation with good constraint satisfaction and momentum and energy-conservation properties. Although originally for conservative systems, variational integrators have been extended to damped systems and continuum mechanics [38], with connections made to widely-used implicit Runge-Kutta schemes [23]. Recent efforts have extended variational integrators to robotics in the context of multibody simulation with contact [39]. However, variational integrators remain an unconventional method for physics simulation, which we partly attribute to their configuration-only representation. Therefore, we extend the variational integrator to a fluid-robot multiphysics setting with full robot-state representations found in standard robotics simulators [34].

In the context of fluid dynamics, variational principles have long been studied [40], [41] to pose fluid physics as continuous-time optimization problems. This optimization-based treatment has inspired several practices in CFD, including the treatment of boundary conditions as constraints with associated dual variables [24], [42], [43]. Holm [44] has also extended variational principles to the stochastic fluids setting.

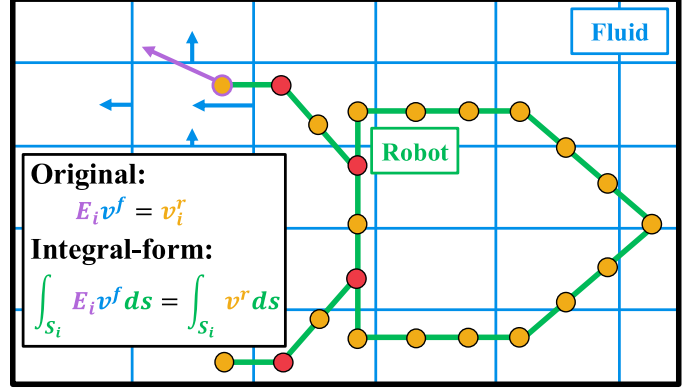


Fig. 5: The immersed-boundary method, where the fluid domain and robot geometry are discretized separately into a grid and boundary-mesh. Originally, the fluid-robot interface is modeled by a convolution matrix  $E$  that maps fluid-cell velocities (blue) to those at the robot-boundary nodes (orange). This can lead to fluid-penetration and singularities at duplicate nodes (red) that correspond to multiple bodies. Therefore, we introduce an extension integrates the immersed boundary method across the boundary (green), improving both physical accuracy and compatibility with multibody representations, which are common in robotics.

We aim to extend these variational principles to the discrete setting with robot dynamics in mind, resulting in naturally-coupled multiphysics simulation.

## III. BACKGROUND

This section provides a brief overview of variational calculus, variational integrators, and the immersed boundary method for fluid-structure interaction. We refer the reader to the comprehensive, existing literature for more details [23]–[25], [40], [41].

### A. Physics as Optimization

Various differential equations for modeling physics can be derived from the principle of least action via variational calculus. Specifically, the principle of least action represents the dynamics as a continuous-time optimization problem:

$$\begin{aligned} & \underset{q, v}{\text{minimize}} && \int_{t_0}^{t_f} T(v(t)) - U(q(t)) dt \\ & \text{subject to} && v = \dot{q}, \end{aligned} \quad (1)$$

where  $q(t) \in \mathbb{R}^n$  is the configuration of the system (e.g., fluid-particle position and robot pose) as a function of time,  $t$ ;  $v(t) \in \mathbb{R}^m$  is the velocity;  $T(v) \in \mathbb{R}^+$  is the kinetic energy of the system; and  $U(q) \in \mathbb{R}^+$  is the potential energy; and  $v = \dot{q}$  represents the kinematic constraint. We denote  $L(q, v) = T(v) - U(q)$  as the *physics* Lagrangian, which we can use to derive an expression for the action,

$$S(q, v) = \int_{t_0}^{t_f} L(q, v) + \lambda^T (\dot{q} - v) dt. \quad (2)$$

where  $\lambda$  is the dual variable. The first-order necessary (FON) conditions of the optimization problem posed by (1) are subsequently solved to derive the Euler-Lagrange equation that governs the system dynamics:

$$\frac{d}{dt} \frac{\partial L}{\partial \dot{q}} - \frac{\partial L}{\partial q} = 0, \quad (3)$$

which is commonly rewritten as the manipulator equation in robotics:

$$M(q)\ddot{q} + C(q, \dot{q})\dot{q} + G(q) = 0. \quad (4)$$

We note that the least-action principle can be extended to non-conservative systems via the Lagrange-D'Alembert principle of virtual work [38]; to more complex kinematics  $v = f(q, \dot{q})$  as encountered e.g. with different parametrizations of attitude [45]; and to include constraints such as joint constraints in manipulator arms [46]. This provides a more complete least-action principle:

$$\begin{aligned} & \underset{q, v}{\text{minimize}} && \int_{t_0}^{t_f} T(q, v) - U(q) + F(t)^T q(t) dt \\ & \text{subject to} && v = f(q, \dot{q}), \\ & && c(q, v) = 0, \end{aligned} \quad (5)$$

where  $F(t) \in \mathbb{R}^n$  represents external forces such as damping.

### B. Variational Integrators

Robotics simulators commonly integrate (4) via a Runge-Kutta (RK) scheme to simulate a system [34]. However, most RK schemes are known to exhibit unstable behavior or introduce artificial damping, introducing a sim-to-real gap. Meanwhile, variational integrators provide implicit time-integration schemes that are known to conserve energy and momentum, making them attractive for robotics simulators.

First, the continuous-time action integral is discretized via numerical quadrature. As a particular example shown in Figure 4, a midpoint quadrature rule results in the following optimization problem:

$$\begin{aligned} & \underset{q_k}{\text{minimize}} && \sum_{k=1}^2 L_d(q_k, q_{k+1}) + \frac{h}{2} F(t_k + \frac{h}{2})^T (q_k + q_{k+1}) \\ & \text{subject to} && c(q_k) = 0, \end{aligned} \quad (6)$$

where  $q_k$  is the configuration at time  $t_k$ ;  $h \in \mathbb{R}$  is the time step; and  $L_d(q_k, q_{k+1}) \in \mathbb{R}^+$  is the discrete Lagrangian, which is expressed as:

$$L_d(q_k, q_{k+1}) = hL\left(\underbrace{\frac{q_k + q_{k+1}}{2}}_{\bar{q}_{k+1}}, \underbrace{\frac{q_{k+1} - q_k}{h}}_{\bar{v}_{k+1}}\right) \quad (7)$$

where  $\bar{q}_{k+1}$  and  $\bar{v}_{k+1}$  are the configurations and velocities defined at the midpoint between  $t_k$  and  $t_{k+1}$ .

We then obtain the discrete Euler-Lagrange equation, which is the FON condition of (6) w.r.t.  $q_k$ :

$$\begin{aligned} & D_2 L_d(q_{k-1}, q_k) + D_1 L_d(q_k, q_{k+1}) \\ & + h\bar{F}_k + h \underbrace{\lambda_k^T D_1 c(q_k)}_{\text{constraint force}} = 0, \end{aligned} \quad (8)$$

$$c(q_{k+1}) = 0, \quad (9)$$

where  $\lambda_k \in \mathbb{R}^z$  is the dual variable. Upon inspection,  $\lambda_k$  provides an impulse over  $t_k$  to  $t_{k+1}$  to enforce the constraint  $c(q_{k+1}) = 0$ .  $D_k$  denotes partial differentiation with respect to a function's  $k$ th argument, and  $\bar{F}_k$  represents the averaged external force  $F(t)$  at the midpoint:

$$\bar{F}_k = \frac{1}{2}(F(t_k - \frac{h}{2}) + F(t_k + \frac{h}{2})). \quad (10)$$

By initializing  $q_k$  and  $q_{k-1}$ , (8)-(9) can be solved to compute  $q_{k+1}$ . However, this integration method only integrates over configurations, with a half-time-step delay present between  $q_k$  and  $\bar{v}_k$ . This introduces a temporal inconsistency due to the fluid being modeled as a velocity field,  $\bar{v}_k(q_k)$ , while the robot's pose is defined by  $q_k$ . Marsden et al. [23] previously connected this variational integrator to the implicit midpoint RK scheme over the full state,  $x = [q; v]$ , via the discrete Legendre transform. However, doing so with constraints can be difficult and unintuitive. Therefore, we aim to provide a simpler approach for performing variational integration over the full midpoint state,  $\bar{x} = [\bar{q}; \bar{v}]$ , to ensure a temporally-consistent fluid-robot representation.

### C. The Immersed Boundary Method

To account for the representation discrepancy between the Eulerian fluid-velocity grid and Lagrangian (free-floating) robot geometry, Peskin [25] formulated the immersed boundary method to model the no-slip boundary condition at the robot-fluid interface as shown in Figure 5. Specifically, the fluid velocity is set equal to the robot velocity at its boundary, which is expressed as the following integration over the fluid-velocity field:

$$\int_{\Omega} v^f \delta(q^f - {}^b q^r) d\Omega = {}^b v^r \quad \forall {}^b q^r \in \partial\Gamma, \quad (11)$$

where  $\Omega$  is the fluid domain;  $\partial\Gamma$  is the robot geometry's boundary;  $v^f$  is the fluid velocity at position  $q^f$ ;  $q^r, v^r$  are the solid body (i.e., robot) configuration and velocity; and  ${}^b v^r$  is the velocity at a point  ${}^b q^r$  along  $\partial\Gamma$ .  $\delta()$  is the dirac delta function. In addition, the corresponding forcing term acting on the fluid is explicitly defined as an inverse mapping:

$$F^f = \int_{\Gamma} F^r \delta(q^f - {}^b q^r) d\Gamma \quad \forall q^f, \quad (12)$$

In discrete form, the fluid domain and robot geometry are discretized into a separate grid and mesh respectively, allowing for decoupled movement of the robot. Meanwhile, the dirac delta is approximated by a smoothed version. This results in the discretized immersed boundary method:

$$c(v^f, q^r, v^r) = E v_d^f - {}^b v_d^r(q^r, v^r) = 0, \quad (13)$$

$$F_d^f = E^T(q^r) F_d^r, \quad (14)$$

where  $E$  is a convolution matrix that maps discrete fluid velocities on the grid to those of the robot-boundary nodes. However, upon inspection, this discretized constraint is only satisfied at finite nodes of the boundary mesh, allowing fluid to penetrate the boundary if the nodes are far apart. On

the other hand, overlapping points can cause numerical ill-conditioning due to redundant no-slip constraints, which can occur in multibody robots as shown in Figure 5. Therefore, we extend the immersed boundary method to derive an integral-form that will properly enforce no-slip in between nodes while being unaffected by overlapping ones.

#### IV. METHODOLOGY

##### A. Fluid-Robot Multiphysics as Optimization

As previously mentioned, existing simulators [9], [10] typically integrate over the individual differential equations before coupling the physics via a force term such as (12). We propose the least-action principle as an alternative, unified perspective of multiphysics from which the differential equations are derived.

We begin by proposing the least-action principle for the combined multiphysics problem between a rigid (multi)body robot and an incompressible, Newtonian fluid (e.g., water):

$$\begin{aligned} & \underset{q_k^r, q^f, v^r, v^f}{\text{minimize}} && \int_{t_0}^{t_f} L^f(q^f, v^f) + L^r(q^r, v^r) + F(t)^T q^f dt \\ & \text{subject to} && c_1(v^f) = \dot{q}^f - v^f(q^f) = 0 \quad \forall q^f \in \Omega, \\ & && c_2(v^f) = \nabla \cdot v^f = 0 \quad \forall q^f \in \Omega, \\ & && c_3(v^f) = v^f - v_{bc} = 0 \quad \forall q^f \in \partial\Omega, \\ & && c_4(v^r) = \dot{q}^r - v^r = 0 \quad \forall q^r, \\ & && c_5(q^r) = 0 \quad \forall q^r, \\ & && c_6(v^f, v^r) = v^f - {}^b v^r = 0. \quad \forall q^f \in \Gamma \end{aligned} \quad (15)$$

where  $\Omega, \Gamma$  represent the fluid domain and robot geometry respectively with corresponding boundaries,  $\partial\Omega, \partial\Gamma$ ;  $q^r, q^f$  are the configurations of the robot and fluid particle respectively and  $v^r, v^f$  are the corresponding velocities.  $c_1(v^f)$  encodes the kinematics constraint for the fluid-velocity field (i.e., an array of velocity sensors).  $c_2(v^f)$  encodes the conservation-of-mass constraint while  $c_3(v^f)$  enforces boundary conditions along the fluid-domain boundary (e.g., walls, free-stream velocity, etc.).  $c_4(q^r)$  encodes the kinematics constraint of the robot while  $c_5$  enforces other robot-configuration constraints, such as joint constraints found in manipulator arms.  $c_6(v^f, q^r, v^r)$  encodes the no-slip constraint, which couples the robot and fluid physics.

We first define the fluid and (single) rigid-body Lagrangians:

$$L^f(q^f, v^f) = \int_{\Omega} \frac{1}{2} \rho (v^f)^T v^f - \rho g^T q^f dV, \quad (16)$$

$$L^r(q^r, v^r) = \frac{1}{2} (v^r)^T M^r v^r - M^r g^T q^r, \quad (17)$$

where  $\rho$  is the fluid density;  $M$  is the mass matrix of the robot body;  $dV$  denotes the volume differential; and  $g$  is gravity. In this problem, damping is introduced by the fluid viscosity:

$$F(t) = \int_{\Omega} \mu \Delta v^f dV, \quad (18)$$

where  $\mu$  is the dynamic viscosity of the fluid. In a manner similar to (2), we write down the action for combine problem:

$$S(q^r, q^f, v^f, v^r) = \int_{t_0}^{t_f} L^f + L^r + F^T q^f + \sum_{i=1}^6 \lambda_i c_i dt \quad (19)$$

The FON conditions of (15) can be expressed by the variations w.r.t.  $q^r, v^r$  and  $q^f, v^f$ , which results in the coupled incompressible Navier-Stokes and manipulator equations, respectively:

$$\begin{aligned} \rho(\dot{v}^f + (v^f \cdot \nabla)v^f) &= -\nabla p + \mu \nabla^2 v^f - \rho g \\ &\quad - \frac{\partial c_3}{\partial v^f}^T \dot{\lambda}_3 - \frac{\partial c_6}{\partial v^f}^T \dot{\lambda}_6, \end{aligned} \quad (20)$$

$$\nabla \cdot v^f = 0, \quad (21)$$

$$\overbrace{M v^r}^{(4)} + \rho g = \frac{\partial c_5}{\partial q^r}^T \lambda_5 - \frac{\partial c_6}{\partial v^r}^T \dot{\lambda}_6. \quad (22)$$

$$\dot{q}^r = v^r, \quad (23)$$

where  $p = \dot{\lambda}_2 \in R^m$  is the fluidic pressure, which Lagrange [47] originally realized as the dual variable that enforces the conservation of mass. (20) also provides the same constraint-based treatment of fluid-boundary conditions of Allmaras [43]. In similar fashion, the multiphysics-coupling force also corresponds to the no-slip-constraint Jacobian and the respective dual variable,  $\dot{\lambda}_6$ .

##### B. Coupled Discretization of the Fluid-Robot Multiphysics

Using the unified least-action principle of (15), we develop a variational integrator to simulate fluid-robot multiphysics. However, we again note that  $q^r$  and  $v^f$  have a half-time-step lag in traditional variational integrators. Therefore, we aim to derive a new variational integrator whose  $q_k$  and  $v_k$  correspond to the same time,  $t_k$  to maintain temporal consistency.

First, we discretize the fluid domain spatially using a second-order finite-volume method [48], which provides a discrete counterpart to the following continuous operators:

$$\int_{\Omega} \rho v^f dV \Rightarrow M^f v^f, \quad (24)$$

$$\int_{\Omega} (v^f \cdot \nabla) v^f dV \Rightarrow N(v^f), \quad (25)$$

$$\int_{\Omega} \nabla p dV \Rightarrow G p, \quad (26)$$

$$\int_{\Omega} \Delta v^f dV \Rightarrow L v^f. \quad (27)$$

Through a slight abuse of notation, we will use  $q^f, v^f$ , and  $p$  to refer to their discrete versions throughout the rest of this section. We may now express the spatially discrete fluid Lagrangian as:

$$L^f(q^f, v^f) = \frac{1}{2} (v^f)^T M^f v^f - M^f g^T q^f dV, \quad (28)$$

We then note that  $\bar{q}_k, \bar{v}_k$  are both defined at the same time,  $t_k - \frac{h}{2}$ . Therefore, we express all the constraints of (15) to be satisfied at the midpoints, resulting in the following discretized action:

$$\begin{aligned} & \underset{q_k^r, q_k^f}{\text{minimize}} && \sum_{k=1}^2 L_d^f(q_k^f, q_{k+1}^f) + L_d^r(q_k^r, q_{k+1}^r) + h \bar{F}_k \\ & \text{subject to} && c_2(\bar{v}_k^f) = G^T \bar{v}_k^f = 0, \\ & && c_3(\bar{v}_k^f) = B \bar{v}_k^f - v_{bc} = 0, \\ & && c_5(\bar{q}_k^r) = 0, \\ & && c_6(\bar{v}_k^f, \bar{v}_k^r) = E \bar{v}_k^f - {}^b \bar{v}^r(\bar{v}_k^r) = 0, \end{aligned} \quad (29)$$

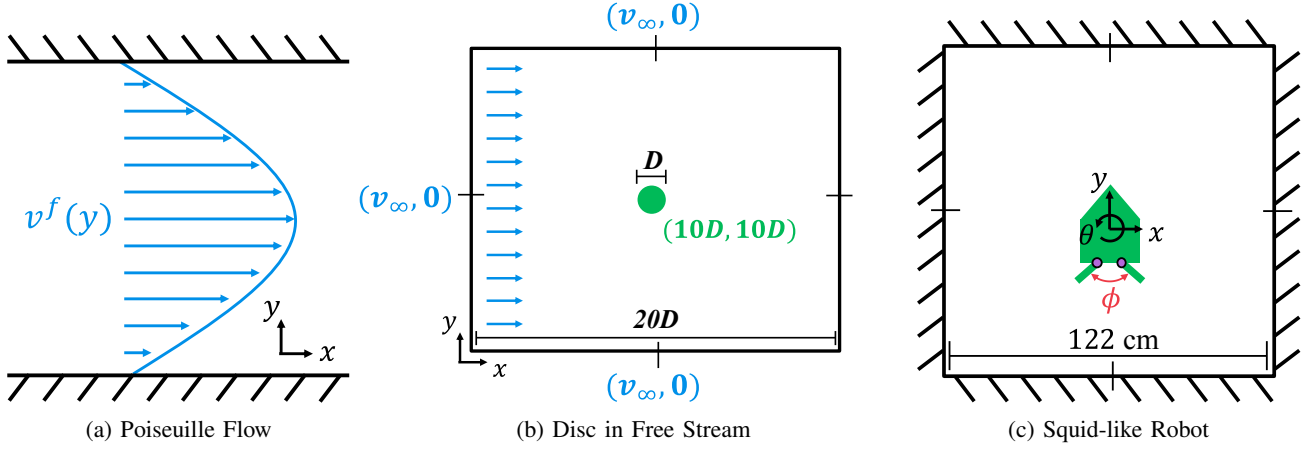


Fig. 6: Experiment setups for benchmarking our unified fluid-robot multiphysics approach. A Poiseuille-flow environment is simulated to benchmark the fluid-boundary conditions and resulting fluid-velocity profile to ground truth. A disc-in-free-stream simulation is used to benchmark the resulting drag and lift forces acting on a solid body in various Reynold's numbers. The fully-coupled fluid-robot dynamics is then realized with the simulation of a squid-like swimming robot before being replicated on real-world hardware for comparison.

where  $B\bar{v}_k^f$  extracts fluid velocities located at the fluid-domain boundary, and  $c_6(\bar{v}^f, \bar{v}^r)$  is expressed using the discretized immersed boundary method posed in (13). The external force is additionally modified to account for the convective term defined by (25):

$$\bar{F}_k = \frac{1}{2}(\mu L \bar{v}_k^f + N(\bar{v}_k^f) + \mu L \bar{v}_{k+1}^f + N(\bar{v}_{k+1}^f)). \quad (30)$$

Upon inspection, we note that the slot derivatives of (8) can be expressed in terms of  $\bar{q}^f$  and  $\bar{v}^r$  using the chain rule:

$$D_2 L_d(q_{k-1}, q_k) = h \left( \underbrace{\frac{\partial L}{\partial \bar{q}_k}}_{\frac{1}{2}} \frac{\partial \bar{q}_k}{\partial q_k} + \underbrace{\frac{\partial L}{\partial \bar{v}_k}}_{\frac{1}{h}} \frac{\partial \bar{v}_k}{\partial q_k} \right), \quad (31)$$

$$D_1 L_d(q_k, q_{k+1}) = h \left( \underbrace{\frac{\partial L}{\partial \bar{q}_{k+1}}}_{\frac{1}{2}} \frac{\partial \bar{q}_{k+1}}{\partial q_k} + \underbrace{\frac{\partial L}{\partial \bar{v}_{k+1}}}_{-\frac{1}{h}} \frac{\partial \bar{v}_{k+1}}{\partial q_k} \right). \quad (32)$$

We can now substitute (31)-(32) into (8). This results in the following FON conditions for (29) corresponding to the robot dynamics:

$$\bar{q}_{k+1}^r - \frac{h}{2} \bar{v}_{k+1}^r = \bar{q}_k^r + \frac{h}{2} \bar{v}_k^r, \quad (33)$$

$$\begin{aligned} \frac{1}{2} M^r \bar{v}_{k+1}^r + h \left( \frac{\partial c_5}{\partial \bar{q}_k^r} + \frac{\partial c_5}{\partial \bar{q}_{k+1}^r} \right)^T \lambda_{5,k} \\ + \left( \frac{\partial c_6}{\partial \bar{v}_k^r} + \frac{\partial c_6}{\partial \bar{v}_{k+1}^r} \right)^T \lambda_{6,k} = \frac{1}{2} M^r \bar{v}_k^r - h M^r g, \end{aligned} \quad (34)$$

as well as that corresponding to the fluid dynamics:

$$\begin{aligned} \frac{1}{2} (M^f - \mu h L) \bar{v}_{k+1}^f - \frac{h}{2} N(\bar{v}_{k+1}^f) \\ + G p_k + B \lambda_{3,k} + \left( \frac{\partial c_6}{\partial \bar{v}_k^f} + \frac{\partial c_6}{\partial \bar{v}_{k+1}^f} \right)^T \lambda_{6,k} \\ = \frac{1}{2} (M^f + \mu h L) \bar{v}_k^f + \frac{h}{2} N(\bar{v}_k^f) - h M^f g. \end{aligned} \quad (35)$$

Finally, the constraints of (29) form the rest of the FON conditions:

$$G^T \bar{v}_k^f = 0, \quad (36)$$

$$B \bar{v}_k^f - v_{bc} = 0, \quad (37)$$

$$E \bar{v}_k^f - {}^b \bar{v}^r(\bar{v}_k^r) = 0, \quad (38)$$

$$c_5(\bar{q}_k^r) = 0. \quad (39)$$

The system of equations defined by (33)-(39) can be solved using Newton's method. Specifically,  $\bar{q}_{k+1}^r, \bar{v}_{k+1}^r, \bar{v}_{k+1}^f$  and the corresponding dual variables can be solved for given  $\bar{q}_k^r, \bar{v}_k^r, \bar{v}_k^f$ . Upon further inspection, we note that this integration scheme is nearly equivalent to implicit Crank-Nicholson: a stable, energy-preserving RK method commonly used to integrate partial differential equations.

### C. An Integral-Form Immersed Boundary Method

As previously mentioned, the immersed boundary method can be both ill-posed and ill-conditioned due to enforcing the no-slip constraint at a set of (possibly changing) discrete node locations. Therefore, we propose a new formulation that integrates the original immersed boundary method along the solid-body boundary as shown in Figure 5:

$$\oint_{\Gamma} \int_{\Omega} v^f \delta(q^f - {}^b q^r(q^r)) dV dS = \oint_{\Gamma} {}^b v^r(q^r, v^r) dS, \quad (40)$$

where  $\oint dS$  denotes a surface integral. We discretize (40) with piecewise-linear interpolation of the boundary. The discrete delta function is then integrated along each linear interpolant, resulting in another convolution matrix for the following discretized immersed boundary method:

$$\bar{E} v^f - {}^b v^r(v^r) = 0, \quad (41)$$

where  $\bar{E}$  is the integrated convolution matrix. Rather than explicitly formulating a forcing term such as (12), we simply differentiate through (41) as seen in (34)-(35).

## V. EXPERIMENTAL RESULTS

This section presents the results of several validation studies to evaluate our fluid-robot multiphysics approach, which are detailed in Figure 6. These include a Poiseuille-flow simulation to benchmark the fluid-boundary conditions and resulting fluid-velocity profile to ground truth. A disc-in-free-stream simulation is used to benchmark the resulting drag and lift forces acting on a solid body in various Reynold's numbers.

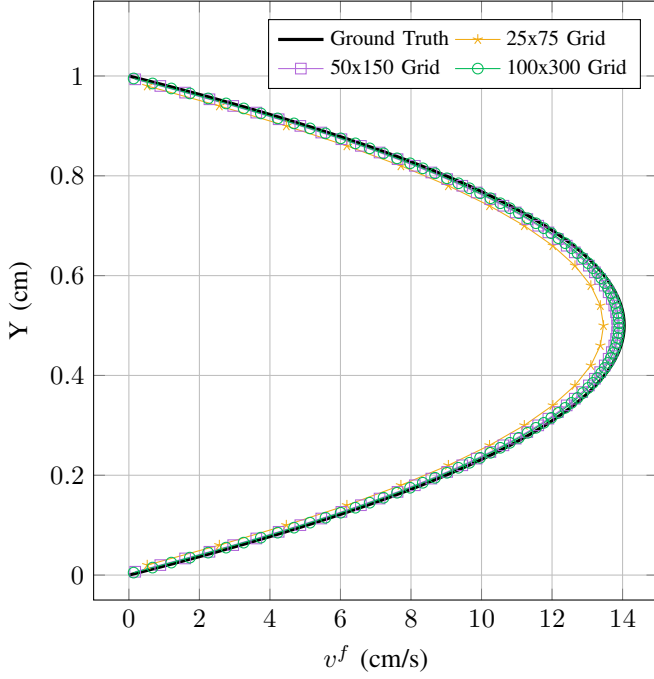


Fig. 7: Steady-state velocity profiles of water under Poiseuille flow across various spatial fidelity. Our variational-integrator approach is able to properly model the wall and periodic boundary conditions to achieve a steady-state fluid-velocity profile that converges to the theoretical ground truth.

The fully-coupled fluid-robot dynamics is then realized with the simulation of a squid-like robot performing a forward-swimming gait, whose trajectory is compared to that of real-world hardware.

#### A. Poiseuille Flow

We first benchmark the discrete fluid dynamics in our variational setup through a Poiseuille-flow simulation as depicted in Figure 6a, which has a known steady-state ground-truth solution. The flow environment is defined as a rectangular grid, whose wall and periodic boundary conditions are simulated as constraints in (29). As shown in Figure 7, our approach converges to the theoretical ground truth with increasing spatial fidelity, demonstrating the efficacy of variational integrators for simulating incompressible fluid dynamics with Eulerian grid representations.

#### B. A Disc in Free Stream

We additionally benchmark our unified framework’s ability to properly simulate lift and drag forces that arise from the fluid-robot interaction. Specifically, we simulate a disc in a free stream environment as depicted in Figure 6b over a  $250 \times 250$  square fluid grid. The no-slip condition is modeled using our integral-form immersed boundary formulation with a mesh fidelity similar to that of the fluid. An additional constraint is modeled in (39) to keep the disc fixed. As shown in Figure 8, our framework is able to properly simulate the corresponding fluid-flow vortices at both low and intermediate Reynold’s numbers. We additionally compare our drag-coefficient values

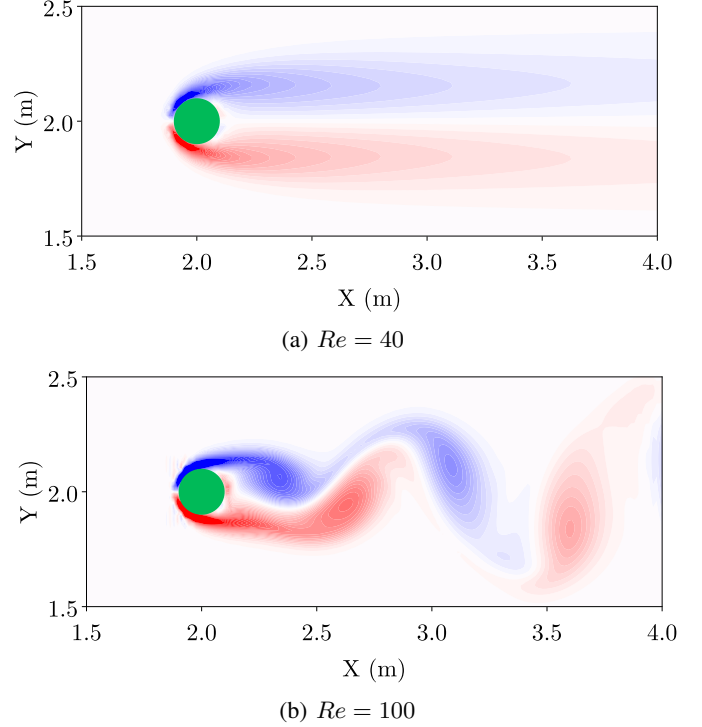


Fig. 8: Vorticity contours of the fully-developed flow around a disc in free-stream conditions at various Reynold’s numbers. Our variational approach is able to properly model the vortex shedding at higher Reynold’s number flows that is consistent with those of incompressible Navier-Stokes solvers.

TABLE I: Steady-state-flow results at  $Re = 40$

|                                   | Drag Coeff. |
|-----------------------------------|-------------|
| Tritton [49] ( <i>empirical</i> ) | 1.65        |
| Taira et. al [24]                 | 1.55        |
| Ren et. al [50]                   | 1.57        |
| Aquarium [33]                     | 1.75        |
| <b>Integral-form IB</b>           | 1.68        |

TABLE II: Fully-developed-flow results at  $Re = 100$

|                         | Drag Coeff.       | Lift Coeff. | Strouhal # |
|-------------------------|-------------------|-------------|------------|
| Braza et. al [51]       | $1.325 \pm 0.008$ | $\pm 0.280$ | 0.164      |
| Ren et. al [50]         | $1.335 \pm 0.011$ | $\pm 0.356$ | 0.164      |
| Aquarium [33]           | $1.481 \pm 0.010$ | $\pm 0.362$ | 0.167      |
| <b>Integral-form IB</b> | $1.439 \pm 0.009$ | $\pm 0.351$ | 0.164      |

to other works in Tables I-II. This includes the original immersed boundary method used in Aquarium [33], which our method improves upon to achieve drag coefficient values that are in good agreement with that of empirical works and other incompressible Navier-Stokes solvers.

#### C. Locomotion of a Squid-like Swimming Robot

We finally validate our framework’s ability to jointly simulate both robot and fluid dynamics. Specifically, we investigate the trajectory of a squid-like robot performing a hand-designed forward-swimming gait in an initially-still-water environment as shown in Figure 6c. An untethered, self-contained robot was designed and fabricated as shown in Figure 9, and the

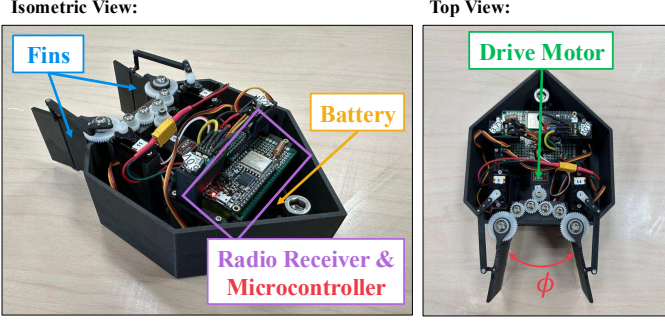


Fig. 9: A real-world squid-like swimming robot designed from the ground up to be untethered with an onboard battery, microcontroller, and transceiver. In this study, the robot receives motor commands over radio to drive the fins to the desired angle,  $\phi$ .

simulation environment is recreated in a real-world setup as shown in Figure 10. Specifically, a square fluid environment was discretized into a  $100 \times 100$  grid with wall boundary conditions. The controls are defined as the angle between the robot fins at each timestep,  $\phi_k$ .

As seen in Figure 1, our multiphysics approach is able to simulate the forward-swimming locomotion behavior, which is consistent with open-loop demonstrations on hardware. Specifically, our framework achieves an RMSE error of 0.89 cm over the whole trajectory. Meanwhile, Genesis [10], a state-of-the-art multiphysics simulator for robotics, has difficulty simulating the fluid-robot interaction to achieve forward motion, resulting in an RMSE error of 8.86 cm over which our framework improves by nearly 90%. We attribute this to Genesis’s particle-based representation of the fluid [15], [29]. We additionally note that the simulation results are achieved with our weak-form immersed boundary method, with the classical formulation failing to simulate the system at all. However, our multiphysics approach predicts a faster swimming gait than that seen on hardware; we attribute this sim-to-real gap to unmodeled 3D effects and mismatch in model parameters (e.g., mass).

## VI. LIMITATIONS

Our unified framework for modeling strongly-coupled multiphysics has several limitations. First, the computational complexity of performing implicit time integration is high, especially when extended to 3D. Future work is needed to develop efficient sparsity-exploiting solvers to scale our method to large-scale problems. Additionally, while the Eulerian fluid representation is well suited for robotic tasks like swimming, it is less convenient for visual rendering than particle-based methods. Finally, our integral-form immersed boundary method still suffers from some artifacts inherent to classical immersed-boundary methods, such as the presence of fluid in the interior of bodies [52], [53].

## VII. CONCLUSION

We have presented a unified framework for deriving and simulating fluid-robot multiphysics as a single optimization

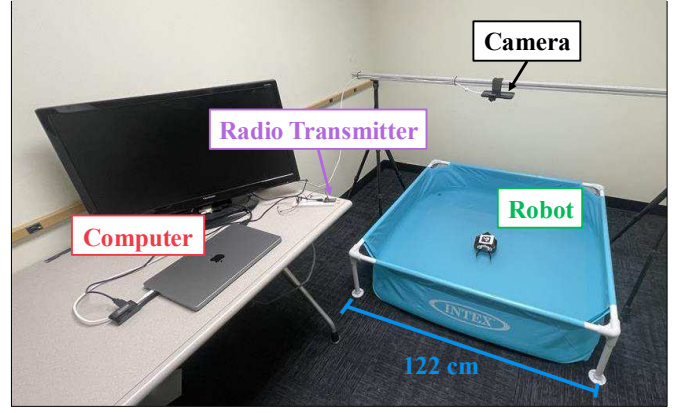


Fig. 10: Hardware-experiment setup for sim-to-real validation of a squid-like robot swimming in an initially-still-water environment. A computer sends motor commands over radio to the robot to execute an undulating, forward-swimming gait. The robot-configuration trajectory is tracked by a top-down-facing camera via an aruco marker.

problem. Specifically, we model the unified least-action principle from which the coupled differential equations are derived. We build upon previous works in variational mechanics to discretize the action directly to simulate the fluid-robot interaction in a stable, tightly-coupled manner. We additionally modify the original immersed boundary method to be amenable to multi-body systems found in robotics. The result is good agreement with both classical fluid-dynamics benchmark problems and real-world rollouts on a bioinspired robot.

In future work, we aim to address the current limitations of our variational method for downstream design and trajectory optimization tasks. We also wish to explore the connections to other CFD methods like implicit large-eddy simulations. Finally, we hope to extend our framework to other multiphysics problems such as rigid-soft robots that experience contact.

## REFERENCES

- [1] Z. Xu, C. Chi, B. Burchfiel, E. Cousineau, S. Feng, and S. Song, “Dex-tAIRity: Deformable Manipulation Can be a Breeze,” 2022. [eprint: 2203.01197](#).
- [2] H. Shi, H. Xu, S. Clarke, Y. Li, and J. Wu, “Robocook: Long-horizon elasto-plastic object manipulation with diverse tools,” *arXiv preprint arXiv:2306.14447*, 2023.
- [3] U. Yoo, A. Hung, J. Francis, J. Oh, and J. Ichnowski, “RoPotter: Toward Robotic Pottery and Deformable Object Manipulation with Structural Priors,” in *2024 IEEE-RAS 23rd International Conference on Humanoid Robots (Humanoids)*, pp. 843–850, IEEE, 2024.
- [4] A. LaGrassa, M. Lee, and O. Kroemer, “Task-Oriented Active Learning of Model Preconditions for Inaccurate Dynamics Models,” 2024. [eprint: 2401.04007](#).
- [5] J. Ichnowski, Y. Avigal, Y. Liu, and K. Goldberg, “Gomp-fit: Grasp-optimized motion planning for fast inertial transport,” in *2022 international conference on robotics and automation (ICRA)*, pp. 5255–5261, IEEE, 2022.
- [6] Z. Yang, M. N. Saadatzi, R. Zhang, A. Sherehiy, D. Wei, C. K. Harnett, and D. O. Popal, “Multiphysics Dynamic Model Validation Methodology for Laser-Driven Microrobots,” in *2019 IEEE 15th International Conference on Automation Science and Engineering (CASE)*, pp. 1555–1561, 2019.
- [7] D. Costa, G. Palmieri, M.-C. Palpacelli, D. Scaradozzi, and M. Callegari, “Design of a Carangiform Swimming Robot through a Multiphysics Simulation Environment,” *Biomimetics (Basel, Switzerland)*, vol. 5, Sept. 2020. Place: Switzerland.

- [8] M. O'Connell, G. Shi, X. Shi, K. Azizzadenesheli, A. Anandkumar, Y. Yue, and S.-J. Chung, "Neural-Fly enables rapid learning for agile flight in strong winds," *Science Robotics*, vol. 7, no. 66, p. eabm6597, 2022. [\\_eprint: https://www.science.org/doi/pdf/10.1126/scirobotics.abm6597](https://www.science.org/doi/pdf/10.1126/scirobotics.abm6597).
- [9] M. Macklin, "Warp: A High-performance Python Framework for GPU Simulation and Graphics," Mar. 2022.
- [10] G. Authors, "Genesis: A Universal and Generative Physics Engine for Robotics and Beyond," Dec. 2024.
- [11] A. P. Maertens, A. Gao, and M. S. Triantafyllou, "Optimal undulatory swimming for a single fish-like body and for a pair of interacting swimmers," *Journal of Fluid Mechanics*, vol. 813, pp. 301–345, 2017. Publisher: Cambridge University Press.
- [12] A. Gao and M. S. Triantafyllou, "Independent caudal fin actuation enables high energy extraction and control in two-dimensional fish-like group swimming," *Journal of Fluid Mechanics*, vol. 850, pp. 304–335, 2018. Publisher: Cambridge University Press.
- [13] G. Novati, S. Verma, D. Alexeev, D. Rossinelli, W. M. Van Rees, and P. Koumoutsakos, "Synchronisation through learning for two self-propelled swimmers," *Bioinspiration & biomimetics*, vol. 12, no. 3, p. 036001, 2017. Publisher: IOP Publishing.
- [14] R. K. Katzschmann, J. DelPreto, R. MacCurdy, and D. Rus, "Exploration of underwater life with an acoustically controlled soft robotic fish," *Science Robotics*, vol. 3, no. 16, p. eaar3449, 2018.
- [15] J. G. Miles and N. A. Battista, "Don't be jelly: Exploring effective jellyfish locomotion," *arXiv preprint arXiv:1904.09340*, 2019.
- [16] Y. Jiao, F. Ling, S. Heydari, N. Heess, J. Merel, and E. Kanso, "Learning to swim in potential flow," *Physical Review Fluids*, vol. 6, May 2021. Publisher: American Physical Society (APS).
- [17] M. Triantafyllou and G. Triantafyllou, "An Efficient Swimming Machine," *Scientific American - SCI AMER*, vol. 272, pp. 64–70, Mar. 1995.
- [18] M. S. Triantafyllou, G. S. Triantafyllou, and D. K. P. Yue, "Hydrodynamics of Fishlike Swimming," *Annual Review of Fluid Mechanics*, vol. 32, no. 1, pp. 33–53, 2000.
- [19] D. N. BEAL, F. S. HOVER, M. S. TRIANTAFYLLOU, J. C. LIAO, and G. V. LAUDER, "Passive propulsion in vortex wakes," *Journal of Fluid Mechanics*, vol. 549, pp. 385–402, 2006.
- [20] J. M. ANDERSON, K. STREITLIEN, D. S. BARRETT, and M. S. TRIANTAFYLLOU, "Oscillating foils of high propulsive efficiency," *Journal of Fluid Mechanics*, vol. 360, pp. 41–72, 1998.
- [21] J. M. Anderson and N. K. Chhabra, "Maneuvering and stability performance of a robotic tuna," *Integrative and comparative biology*, vol. 42, pp. 118–126, Feb. 2002.
- [22] C. Christianson, Y. Cui, M. Ishida, X. Bi, Q. Zhu, G. Pawlak, and M. Tolley, "Cephalopod-inspired robot capable of cyclic jet propulsion through shape change," *Bioinspiration & biomimetics*, vol. 16, Sept. 2020.
- [23] J. Marsden and M. West, "Discrete mechanics and variational integrators," *Acta Numerica*, pp. 357–514, 2001.
- [24] K. Taira and T. Colonius, "The immersed boundary method: A projection approach," *Journal of Computational Physics*, vol. 225, no. 2, pp. 2118–2137, 2007.
- [25] C. S. Peskin, "The immersed boundary method," *Acta numerica*, vol. 11, pp. 479–517, 2002.
- [26] Y. Qiao, J. Liang, V. Koltun, and M. Lin, "Differentiable simulation of soft multi-body systems," *Advances in Neural Information Processing Systems*, vol. 34, pp. 17123–17135, 2021.
- [27] Z. Xian, B. Zhu, Z. Xu, H.-Y. Tung, A. Torralba, K. Fragkiadaki, and C. Gan, "FluidLab: A Differentiable Environment for Benchmarking Complex Fluid Manipulation," 2023. [\\_eprint: 2303.02346](https://arxiv.org/abs/2303.02346).
- [28] M. Macklin, M. Müller, N. Chentanez, and T.-Y. Kim, "Unified particle physics for real-time applications," *ACM Trans. Graph.*, vol. 33, July 2014. Place: New York, NY, USA Publisher: Association for Computing Machinery.
- [29] Y. Hu, Y. Fang, Z. Ge, Z. Qu, Y. Zhu, A. Pradhana, and C. Jiang, "A moving least squares material point method with displacement discontinuity and two-way rigid body coupling," *ACM Transactions on Graphics (TOG)*, vol. 37, no. 4, pp. 1–14, 2018. Publisher: ACM New York, NY, USA.
- [30] F. Palacios, T. D. Economou, A. Aranake, S. R. Copeland, A. K. Lonkar, T. W. Lukaczky, D. E. Manosalvas, K. R. Naik, S. Padron, B. Tracey, and others, "Stanford university unstructured (SU2): Analysis and design technology for turbulent flows," in *52nd Aerospace Sciences Meeting*, p. 0243, 2014.
- [31] E. Nava, J. Z. Zhang, M. Y. Michelis, T. Du, P. Ma, B. F. Grewe, W. Matusik, and R. K. Katzschmann, "Fast Aquatic Swimmer Optimization with Differentiable Projective Dynamics and Neural Network Hydrodynamic Models," in *International Conference on Machine Learning*, pp. 16413–16427, PMLR, 2022.
- [32] W. Liu, K. Bai, X. He, S. Song, C. Zheng, and X. Liu, "FishGym: A High-Performance Physics-based Simulation Framework for Underwater Robot Learning," *arXiv preprint arXiv:2206.01683*, 2022.
- [33] J. H. Lee, M. Y. Michelis, R. Katzschmann, and Z. Manchester, "Aquarium: A Fully Differentiable Fluid-Structure Interaction Solver for Robotics Applications," in *2023 IEEE International Conference on Robotics and Automation (ICRA)*, pp. 11272–11279, 2023.
- [34] E. Todorov, T. Erez, and Y. Tassa, "MuJoCo: A physics engine for model-based control," in *2012 IEEE/RSJ International Conference on Intelligent Robots and Systems*, pp. 5026–5033, 2012.
- [35] T. Du, K. Wu, A. Spielberg, W. Matusik, B. Zhu, and E. Sifakis, "Functional optimization of fluidic devices with differentiable stokes flow," *ACM Transactions on Graphics (TOG)*, vol. 39, no. 6, pp. 1–15, 2020. Publisher: ACM New York, NY, USA.
- [36] J. Grover, J. Zimmer, T. Dear, M. Travers, H. Choset, and S. D. Kelly, "Geometric Motion Planning for a Three-Link Swimmer in a Three-Dimensional low Reynolds-Number Regime," in *2018 Annual American Control Conference (ACC)*, pp. 6067–6074, 2018.
- [37] J. Grover and D. Vedova, "Motion planning, design optimization and fabrication of ferromagnetic swimmers," in *Robotics science and systems*, 2019.
- [38] A. Lew, J. E. Marsden, M. Ortiz, and M. West, "An overview of variational integrators," *Finite element methods*, pp. 98–115, 1970.
- [39] T. A. Howell, S. Le Cleac', J. Z. Kolter, M. Schwager, and Z. Manchester, "Dojo: A Differentiable Simulator for Robotics," 2022.
- [40] V. I. Arnold and B. A. Khesin, *Topological methods in hydrodynamics*, vol. 19. Springer, 2009.
- [41] R. L. Seliger and G. B. Whitham, "Variational principles in continuum mechanics," *Proceedings of the Royal Society of London. Series A. Mathematical and Physical Sciences*, vol. 305, no. 1480, pp. 1–25, 1968. Publisher: The Royal Society London.
- [42] T. C. Papanastasiou, N. Malamataris, and K. Ellwood, "A new outflow boundary condition," *International Journal for Numerical Methods in Fluids*, vol. 14, no. 5, pp. 587–608, 1992. [\\_eprint: https://onlinelibrary.wiley.com/doi/pdf/10.1002/fld.1650140506](https://onlinelibrary.wiley.com/doi/pdf/10.1002/fld.1650140506).
- [43] S. Allmaras, "Lagrange multiplier implementation of Dirichlet boundary conditions in compressible Navier-Stokes finite element methods," in *17th AIAA Computational Fluid Dynamics Conference*, p. 4714, 2005.
- [44] D. D. Holm, "Variational principles for stochastic fluid dynamics," *Proceedings of the Royal Society A: Mathematical, Physical and Engineering Sciences*, vol. 471, no. 2176, p. 20140963, 2015. Publisher: The Royal Society Publishing.
- [45] B. E. Jackson, K. Tracy, and Z. Manchester, "Planning With Attitude," *IEEE Robotics and Automation Letters*, vol. 6, no. 3, pp. 5658–5664, 2021.
- [46] D. Baraff, "Linear-time dynamics using Lagrange multipliers," Tech. Rep. CMU-RI-TR-95-44, Carnegie Mellon University, 1996.
- [47] J. L. Lagrange, *Mécanique analytique*, vol. 1. Mallet-Bachelier, 1853.
- [48] J. H. Ferziger, M. Perić, and R. L. Street, *Computational methods for fluid dynamics*. springer, 2019.
- [49] D. J. Tritton, "Experiments on the flow past a circular cylinder at low Reynolds numbers," *Journal of Fluid Mechanics*, vol. 6, no. 4, pp. 547–567, 1959. Publisher: Cambridge University Press.
- [50] W. W. Ren, J. Wu, C. Shu, and W. M. Yang, "A stream function-vorticity formulation-based immersed boundary method and its applications," *International Journal for Numerical Methods in Fluids*, vol. 70, no. 5, pp. 627–645, 2012. [\\_eprint: https://onlinelibrary.wiley.com/doi/pdf/10.1002/fld.2705](https://onlinelibrary.wiley.com/doi/pdf/10.1002/fld.2705).
- [51] M. Braza, P. Chassaing, and H. H. Minh, "Numerical study and physical analysis of the pressure and velocity fields in the near wake of a circular cylinder," *Journal of Fluid Mechanics*, vol. 165, pp. 79–130, 1986. Publisher: Cambridge University Press.
- [52] U. Lăcis, K. Taira, and S. Bagheri, "A stable fluid–structure–interaction solver for low-density rigid bodies using the immersed boundary projection method," *Journal of Computational Physics*, vol. 305, pp. 300–318, 2016. Publisher: Elsevier.
- [53] T. Kempe and J. Fröhlich, "An improved immersed boundary method with direct forcing for the simulation of particle laden flows," *Journal of Computational Physics*, vol. 231, no. 9, pp. 3663–3684, 2012.